Biomimetic Model

DOI: 10.1002/ange.201206922

Aromatic Ring Cleavage of 2-Amino-4-*tert*-butylphenol by a Nonheme Iron(II) Complex: Functional Model of 2-Aminophenol Dioxygenases**

*Biswarup Chakraborty and Tapan Kanti Paine**

A large variety of dioxygenases, which catalyze the ring cleavage of aromatic compounds, are found in aerobic bacteria.[1–3] Catechol-cleaving dioxygenases are well-studied examples in this class of enzymes.[1,4–8] *Pseudomonas Pseudoalcaligenes*, which can be found in nitrobenzene-contaminated soil and groundwater, is involved in the catabolism of nitrophenol; the catabolic pathway proceeds through the reduction of 2-nitrophenol to 2-aminophenol.[9,10] Oxidative C–C bond cleavage of 2-aminophenol then forms 2-aminomuconic acid semialdehyde, which spontaneously loses a water molecule to form 2-picolinic acid. In addition, other nitroaromatic compounds are degraded by some bacteria in a similar pathway.[11,12] Furthermore, the metabolism of one of the essential amino acids, tryptophan, proceeds through the formation of 3-hydroxyanthranilate followed by C3–C4 bond cleavage to form quinolinic acid via 2-amino-3-carboxymuconic acid semialdehyde.[13–15]

2-Aminophenol-1,6-dioxygenase (APD),[16–18] isolated and purified from *Pseudomonas Pseudoalcaligenes,* is responsible for the C–C bond cleavage of 2-aminophenols under aerobic conditions (Scheme 1). The degradation of 3-hydroxyanthranilate to quinolinate is catalyzed by 3-hydroxyanthranilate-3,4-dioxygenase (HAD) in the presence of dioxygen (Scheme 1).[19] Structural studies show that the active site of HAD contains an iron(II) center that is coordinated by the "2-His-1-Glu facial triad".[20–22] Both APD and HAD belong to the class of nonheme iron(II) enzymes and share functional similarity with extradiol-cleaving catechol dioxygenases. A mechanism, similar to that of extradiol-cleaving catechol dioxygenases, has been proposed for aromatic C–C bond cleavage of 2-aminophenols (Scheme 1).[19,23]

Despite the existence of a large number of iron complexes with the coordinated 2-aminophenolates in different redox states,[24–30] thus far there is no example of a biomimetic iron(II) complex that exhibits C–C bond cleavage activity of 2-aminophenolate in the presence of dioxygen. Herein, we report the synthesis, characterization, and dioxygen reactivity of a nonheme iron(II) complex, $[(6\text{-}Me_3\text{-}TPA)Fe^{II}(4\text{-}t\text{Bu-}HAP)](ClO_4)$ (**1**·ClO_4), in which 6-Me_3-TPA = tris(6-methyl-2-pyridylmethyl)amine and 4-*t*Bu-HAP = monoanionic 2-amino-4-*tert*-butylphenolate. The oxidative C–C bond cleavage of 2-amino-4-*tert*-butylphenolate on complex **1** mimicking the function of APD and HAD is discussed.

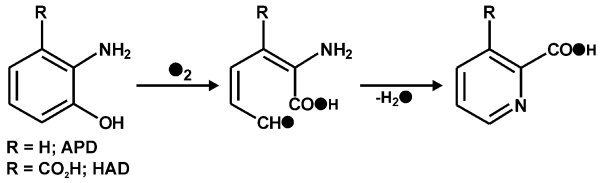

Scheme 1. Reaction catalyzed by APD and HAD.

The iron(II)–2-aminophenolate complex (**1**) was isolated from the reaction of 6-Me_3-TPA ligand, iron(II) perchlorate, and 2-amino-4-*tert*-butylphenol (4-*t*Bu-H_2AP) in the presence of one equivalent of triethylamine in methanol. The yellow solution of complex **1** in acetonitrile displays an intense charge-transfer (CT) band at 404 nm. ^{1}H NMR spectrum of the complex in $CDCl_3$ exhibits paramagnetically shifted proton resonances in the region of −40 ppm to 60 ppm (see Figure S1 in the Supporting Information). The NMR data along with the magnetic moment of 5.1 μ_B at room temperature are indicative of the high-spin nature of the iron(II) complex. Complex **1** was further characterized by single-crystal X-ray diffraction. Unfortunately, all attempts to grow single crystals of **1**·ClO_4 were unsuccessful. However, X-ray-quality single crystals of **1**·BPh_4 (see Experimental Section in the Supporting Information) were isolated from a dichloromethane/methanol/diethyl ether solvent mixture at 273 K.

X-ray crystal structure of the complex cation shows a six-coordinate iron center ligated by four nitrogen donors from the tetradentate ligand, and one nitrogen and one oxygen donor from the aminophenol ligand (Figure 1). The Fe–N_{py} distances are in a range of 2.186(3) Å to 2.305(3) Å, similar to those reported for other high-spin iron(II) complexes of the tetradentate 6-Me_3-TPA ligand.[31,32] The aminophenol ligand binds to the metal center through N5 and O1 with Fe1–N5 and Fe1–O1 distances of 2.282(3) and 1.934(3) Å, respectively (see Table S1 in the Supporting Information). A short Fe1–O1 distance implies a monoanionic binding of the aminophenolate (4-*t*Bu-HAP). Recently, Fiedler and co-workers have reported an iron(II)–aminophenolate complex, $[(Tp^{Ph2})Fe^{II}$-

[*] B. Chakraborty, Dr. T. K. Paine
Department of Inorganic Chemistry
Indian Association for the Cultivation of Science
2A & 2B Raja S. C. Mullick Road, Jadavpur
Kolkata-700032 (India)
E-mail: ictkp@iacs.res.in

[**] T.K.P. acknowledges the DST, Government of India (Project SR/S1/IC-51/2010) for financial support. B.C. thanks CSIR, India, for a fellowship. The crystal-structure determination was performed at the DST-funded National Single Crystal Diffractometer Facility in the Department of Inorganic Chemistry, IACS.

Supporting information for this article is available on the WWW under http://dx.doi.org/10.1002/anie.201206922.

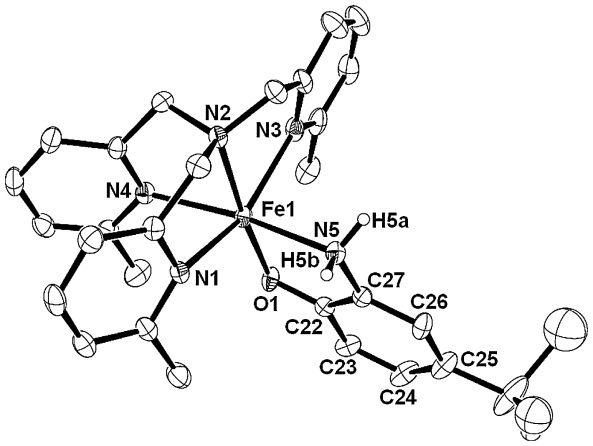

Figure 1. ORTEP plot of the complex cation of $\mathbf{1}\cdot BPh_4$ with 40% thermal ellipsoids. All hydrogen atoms except those on N5 have been omitted for clarity. Selected bond lengths [Å] and angles [deg] for $\mathbf{1}\cdot BPh_4$: Fe1–O1 1.934(3), Fe1–N1 2.305(3), Fe1–N2 2.186(3), Fe1–N3 2.290(3), Fe1–N4 2.256(3), Fe1–N5 2.282(3), C22–O1 1.320(5), C22–C23 1.392(6), C23–C24 1.385(6), C24–C25 1.402(7), C25–C26 1.380(6), C26–C27 1.387(6), C27–C22 1.408(6); O1-Fe1-N1 106.17(12), O1-Fe1-N2 175.29(12), O1-Fe1-N3 102.00(13), O1-Fe1-N4 104.09(12), O1-Fe1-N5 80.55(11), N1-Fe1-N2 77.61(12), N1-Fe1-N3 151.42(13), N1-Fe1-N4 78.57(12), N1-Fe1-N5 88.49(12), N2-Fe1-N3 74.03(12), N2-Fe1-N4 79.27(12), N2-Fe1-N5 96.88(12), N3-Fe1-N4 99.31(12), N3-Fe1-N5 91.44(12), N4-Fe1-N5 167.00(12).

(^{tBu}APH)] (Tp^{Ph2} = hydrotris(3,5-diphenylpyrazolyl)borate and ^{tBu}APH = monoanionic 2-amino-4,6-di-*tert*-butylphenolate), in which the coordinated aminophenolate has been found to exhibit Fe–N_{amine} and Fe–$O_{phenolate}$ distances of 2.214(1) and 1.931(1) Å, respectively.[33] The C–C distances of the HAP ring in $\mathbf{1}\cdot BPh_4$ are found to be similar to those in [(Tp^{Ph2})Fe^{II}(^{tBu}APH)]. The complex cation of $\mathbf{1}\cdot BPh_4$ has structural similarity with the iron(II)–catecholate complex [(6-Me_3-TPA)Fe^{II}(DBCH)](ClO_4) of the 6-Me_3-TPA ligand (DBCH = monoanionic 3,5-di-*tert*-butylcatecholate).[34] The phenolate oxygen (O1) of 4-*t*Bu-HAP and the amine nitrogen (N2) of the supporting ligand occupy the axial plane of the distorted octahedron with the O1-Fe1-N2 angle of 175.3(1)°. The geometry of the cationic part of $\mathbf{1}\cdot BPh_4$ was optimized by DFT calculation with the atomic coordinates obtained from the crystal structure. The calculated bond parameters (Table S1) of the high-spin iron(II) complex ($S=2$) are in good agreement with those obtained experimentally. A Mulliken spin density plot of the optimized geometry (Figure S2) suggests that 94% of the total electron density is localized on the metal center, 4% on the aminophenolate ring, and the rest on the supporting N_4 ligand (Table S2).

The iron(II)–aminophenolate complex ($\mathbf{1}\cdot ClO_4$) reacts with molecular oxygen in acetonitrile under ambient conditions. A light-yellow solution rapidly turns to deep-green within 2 min. During the reaction, the CT band at 404 nm disappears and three new bands at 366 nm, 600 nm, and 934 nm appear rapidly (Figure 2a). A similar spectral change has been observed in the reaction of [(6-Me_3-TPA)Fe^{II}-(DBCH)](ClO_4) with dioxygen, and the origin of the intense CT bands has been attributed to the catecholato-to-iron(III) CT transitions.[34] In analogy to related complexes,[25,29,35] the

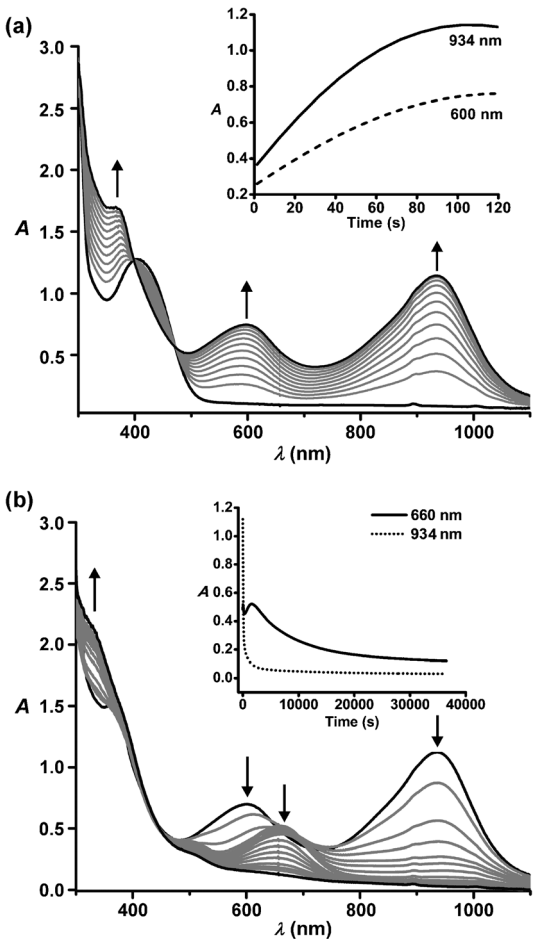

Figure 2. Optical spectral changes over time during the reaction of $\mathbf{1}\cdot ClO_4$ (1 mM solution in acetonitrile, path length = 0.5 cm) with dioxygen at 298 K: a) reaction during the first 2 min, b) slow reaction for 6 h. Inset: plot of absorbance versus time.

CT bands may be assigned to the 2-amidophenolate-to-iron(III) CT transitions. The dark-green solution formed after 2 min shows an EPR signal at $g=4.21$ typical of high-spin iron(III) species with an $S=5/2$ spin state (Figure S3). Additionally, an isotropic signal is also observed at $g=1.99$, possibly because of the presence of a small amount of a radical impurity in the solution. To prove the formation of an iron(III) species in the first step, attempts were made to independently synthesize the iron(III) complex. Unfortunately, no iron(III) complex could be isolated through direct synthesis by mixing the ligand, iron(III) salt, and 2-amino-4-*tert*-butylphenol in the presence of a base. However, controlled one-electron oxidation of $\mathbf{1}\cdot ClO_4$ with a stoichiometric amount of $KMnO_4$ results in the isolation of a dark-green complex, $\mathbf{1}^{ox}\cdot ClO_4$ (Experimental Section). The optical spectral features and the EPR data of $\mathbf{1}^{ox}\cdot ClO_4$ (Figure S4) bear resemblance to those of the deep-green species observed in the reaction of $\mathbf{1}\cdot ClO_4$ with dioxygen. Thus, the initial change in the optical spectrum of $\mathbf{1}\cdot ClO_4$ during the reaction with dioxygen is associated with the formation of [(6-Me_3-TPA)Fe^{III}(4-*t*Bu-AP)](ClO_4) ($\mathbf{1}^{ox}\cdot ClO_4$).

All efforts to isolate the single crystals of $\mathbf{1}^{ox}\cdot ClO_4$ failed. DFT calculations were performed to optimize the geometry

of $[(6\text{-}Me_3\text{-}TPA)Fe^{III}(4\text{-}t\text{Bu-}AP)]^+$ with $S = 5/2$ spin state (Table S3). Time-dependent density functional theory (TDDFT) calculation (Table S4) of the optimized geometry of $[(6\text{-}Me_3\text{-}TPA)Fe^{III}(4\text{-}t\text{Bu-}AP)]^+$ with $S = 5/2$ spin state exhibits three transitions in the 300–1200 nm region (Figure S5), which correlate well with the experimental data. All these results unambiguously confirm a one-electron oxidation of $\mathbf{1}\cdot ClO_4$ with dioxygen in the first step to form an iron(III)–2-imidophenolate species, $\mathbf{1}^{ox}\cdot ClO_4$. A sufficient electron density (Table S3) is observed on 2-imidophenolate ring (19.4%; Figure S2) in the spin density plot of $[(6\text{-}Me_3\text{-}TPA)Fe^{III}(4\text{-}t\text{Bu-}AP)]^+$, which could facilitate further reaction with dioxygen.

In the next step of the reaction with O_2, the CT bands at 934 nm and 600 nm disappear immediately, and a new band appears at 660 nm and subsequently slowly disappears over a period of 6 h, resulting in a light-orange solution (Figure 2b). A similar spectral change is observed upon exposure of a solution of $\mathbf{1}^{ox}\cdot ClO_4$ in acetonitrile to dioxygen for 6 h. During the reaction, the EPR signal at $g = 1.99$ slowly disappears, leaving the high-spin iron(III) signal at $g = 4.21$ after 6 h (Figure S3). The ESI-MS spectrum of the oxidized solution shows an ion signal at $m/z = 566.2$ with the isotope distribution pattern calculated for $[(6\text{-}Me_3\text{-}TPA)Fe(4\text{-}tert\text{-butyl-2-picolinate})]^+$ (Figure 3a, and Figure S6 in the Supporting Information). The formation of picolinate was further confirmed by labeling experiments. ESI-MS of the oxidized solution after reaction of $\mathbf{1}\cdot ClO_4$ with $^{18}O_2$ displays an ion signal at $m/z = 568.2$, thus suggesting the incorporation of one ^{18}O atom into 4-*tert*-butyl-2-picolinate (Figure 3b and Figure S7). Furthermore, the labeling experiment with $H_2{}^{18}O$ and $^{16}O_2$ shows about 30% incorporation of one ^{18}O into the product picolinate (Figure S8).

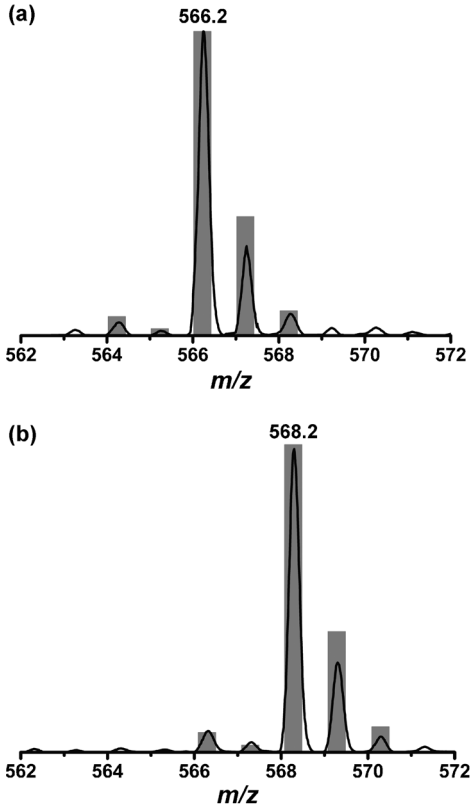

Figure 3. ESI-MS (positive-ion mode in acetonitrile) of the solution after reaction of $\mathbf{1}\cdot ClO_4$ with a) $^{16}O_2$ and b) $^{18}O_2$. The gray bars indicate the corresponding computer-simulated spectra.

The ^1H NMR spectrum of the organic product derived from 2-amino-4-*tert*-butylphenolate shows four distinct and sharp proton resonances; two doublets at 8.6 ppm ($J = 5$ Hz) and 7.4 ppm ($J = 5$ Hz) and two singlets at 8.2 ppm and 1.36 ppm (Figure S9c). The coupling constants of the doublets suggest that the resonances belong to aromatic protons. Of note, a singlet at 6.7 ppm and a multiplet at 6.6 ppm are observed in the ^1H NMR spectrum of the substrate, 2-amino-4-*tert*-butylphenol (Figure S9a). The position of three proton resonances and the coupling constant of the doublets suggest the formation of 4-*tert*-butyl-2-picolinate in the reaction of $\mathbf{1}\cdot ClO_4$ with dioxygen. The absence of a resonance of the aminophenol substrate in the NMR spectrum confirms a complete conversion of 2-amino-4-*tert*-butylphenol to 4-*tert*-butyl-2-picolinic acid in 6 h. To further confirm the conversion, the organic product was analyzed by GC–MS. GC–MS of the methyl ester of the organic product shows an ion signal at $m/z = 193.2$ along with expected fragmentation patterns of methyl-4-*tert*-butyl-2-picolinate (Figure S10). When the reaction is carried out in the presence of $^{18}O_2$, the ion signal at $m/z = 193.2$ is shifted to 195.2, and around 40% incorporation of ^{18}O into methyl-4-*tert*-butyl-2-picolinate is observed (Figure S11). All these results confirm that the reaction of $\mathbf{1}\cdot ClO_4$ with dioxygen leads to the formation of 4-*tert*-butyl-2-picolinic acid through C–C bond cleavage of 2-amino-4-*tert*-butylphenol (Scheme 2) and functionally mimics the reaction catalyzed by 2-aminophenol-1,6-dioxygenase (APD) and 3-hydroxyanthranilate-3,4-dioxygenase (HAD).

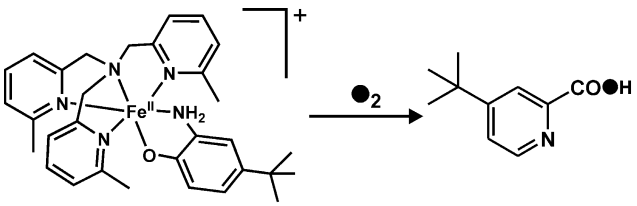

Scheme 2. Reaction of the iron(II)–aminophenolate complex ($\mathbf{1}\cdot ClO_4$) with dioxygen.

To understand the role of the ligand in the oxidative C–C bond cleavage of aminophenolate on the model complex, an equimolar mixture of iron(II) perchlorate, 2-amino-4-*tert*-butylphenol, and triethylamine in acetonitrile was reacted with dioxygen for 6 h. No C–C bond cleavage of 2-amino-4-*tert*-butylphenolate was observed. It is also important to mention here that iron(II) complexes of 2-aminophenol and 2-amino-4,6-di-*tert*-butylphenol, generated in situ in acetonitrile, do not undergo oxidative C–C bond cleavage reactions to afford the corresponding picolinic acid.

The oxidative transformation of 2-amino-4-*tert*-butylphenol to 4-*tert*-butyl-2-picolinic acid takes place through an extradiol-cleavage pathway. Of note, the reaction of an analogous iron(II)–catecholate complex, $[(6\text{-}Me_3\text{-}TPA)Fe^{II}$-

(DBCH)](ClO$_4$), with dioxygen leads to the formation of products of the intradiol-selective C–C bond cleavage of the coordinated catecholate.[34] Moreover, several iron(II)–catecholate complexes of tetradentate ligands have been shown to react with dioxygen to afford mainly products of the intradiol-selective catechol cleavage.[4] Wieghardt and co-workers have reported the synthesis and characterization of a large number of transition-metal complexes of 3,5-di-*tert*-butylaminophenol- and 2-aminophenol-derived ligands.[25–28] The reaction of substituted 2-aminophenolate with an iron(II) salt and a tetradentate ligand (tren) in air resulted in the formation of an iron(III)–2-iminobenzosemiquinonato radical complex.[29] No C–C bond cleavage of aminophenolate has ever been reported to occur during the reaction of transition-metal ions with these ligands.

For iron(II)–catecholate model complexes, the groups of Que and Moro-oka each proposed an outer-sphere one-electron oxidation of iron(II)–catecholate to iron(III)–catecholate species.[36,37] An iron(II)–semiquinone intermediate was proposed to react directly with dioxygen to form an iron(III)–alkylperoxide intermediate for C–C bond cleavage of catecholate.[38] DFT calculations on simplified enzyme–substrate and iron(II)–catecholate model complexes also support that the attack of dioxygen to an iron(II)–semiquinone species is the key step in C–C bond cleavage of catechol.[39,40] Fiedler and co-workers recently isolated and structurally characterized an iron(II)–2-aminophenolate complex, [(Tp^{Ph2})Fe^{II}(^{tBu}APH)], which was converted to an iron(II)–2-iminobenzosemiquinonato radical species upon one-electron chemical oxidation.[33] On the basis of all these observations, it is proposed that complex **1** reacts with dioxygen to undergo one-electron oxidation to form an iron(III)–2-amidophenolate species (**A**) in the first step. The redox isomer of **A**, an iron(II)–2-iminobenzosemiquinonato radical species, then reacts with dioxygen to generate an alkylperoxo intermediate (**B**), leading to the C–C bond cleavage of 2-aminophenol. The resulting extradiol-cleavage product, 2-amino-4-*tert*-butylmuconic acid semialdehyde, then undergoes a cyclization reaction to form 4-*tert*-butyl-2-picolinic acid (Scheme 3).

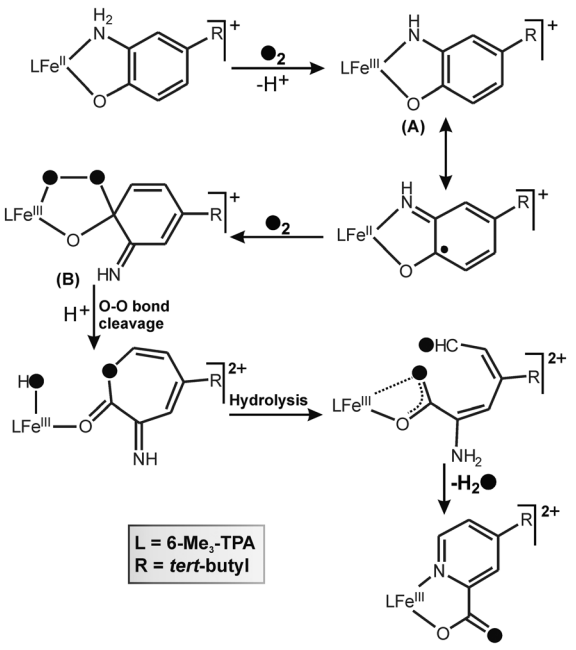

Scheme 3. Proposed pathway for C–C bond cleavage reaction of 2-aminophenolate on **1**·ClO$_4$.

In conclusion, we have synthesized and characterized an iron(II)–2-aminophenolate complex of a tetradentate nitrogen donor ligand. The biomimetic iron(II) complex (**1**) has been shown to react with O_2 to oxidatively cleave the C–C bond of 2-amino-4-*tert*-butylphenol to 4-*tert*-butyl-2-picolinic acid. Complex **1** represents the first functional model of 2-aminophenol dioxygenases, APD and HAD. The extradiol cleavage of 2-amino-4-*tert*-butylphenol reported in this work highlights the importance of the model complex in understanding the unique oxygen-dependent transformation reaction of 2-aminophenol to 2-picolinic acid in a single step, which is unprecedented in synthetic chemistry. A detailed experimental and theoretical investigation on the C–C bond cleavage mechanism of substituted 2-aminophenols by biomimetic iron(II) complexes is presently being pursued in our laboratory.

Received: August 27, 2012
Revised: October 10, 2012
Published online: November 29, 2012

Keywords: biomimetic model · cleavage reactions · dioxygenases · enzyme models · iron

[1] F. H. Vaillancourt, J. T. Bolin, L. D. Eltis, *Crit. Rev. Biochem. Mol. Biol.* **2006**, *41*, 241.
[2] G. Fuchs, M. Boll, J. Heider, *Nat. Rev. Microbiol.* **2011**, *9*, 803.
[3] S. Fetzner, *Appl. Environ. Microbiol.* **2012**, *78*, 2505.
[4] M. Costas, M. P. Mehn, M. P. Jensen, L. Que, Jr., *Chem. Rev.* **2004**, *104*, 939.
[5] E. G. Kovaleva, J. D. Lipscomb, *Science* **2007**, *316*, 453.
[6] T. D. H. Bugg, C. J. Winfield, *Nat. Prod. Rep.* **1998**, *15*, 513.
[7] T. D. H. Bugg, S. Ramaswamy, *Curr. Opin. Chem. Biol.* **2008**, *12*, 134.
[8] J. D. Lipscomb, *Curr. Opin. Struct. Biol.* **2008**, *18*, 644.
[9] C. C. Somerville, S. F. Nishino, J. C. Spain, *J. Bacteriol.* **1995**, *177*, 3837.
[10] S. F. Nishino, J. C. Spain, *Appl. Environ. Microbiol.* **1993**, *58*, 2520.
[11] K.-S. Ju, R. E. Parales, *Microbiol. Mol. Biol. Rev.* **2010**, *74*, 250.
[12] J.-F. Wu, C.-Y. Jiang, B.-J. Wang, Y.-F. Ma, Z.-P. Liu, S.-J. Liu, *Appl. Environ. Microbiol.* **2006**, *72*, 1759.
[13] K. L. Colabroy, T. P. Begley, *J. Bacteriol.* **2005**, *187*, 7866.
[14] K. L. Colabroy, T. P. Begley, *J. Am. Chem. Soc.* **2005**, *127*, 840.
[15] O. Kurnasov, V. Goral, K. Colabroy, S. Gerdes, S. Anantha, A. Osterman, T. P. Begley, *Chem. Biol.* **2003**, *10*, 1195.
[16] U. Lendenmann, J. C. Spain, *J. Bacteriol.* **1996**, *178*, 6227.
[17] S. Takenaka, S. Murakami, R. Shinke, K. Hatakeyama, H. Yukawa, K. Aoki, *J. Biol. Chem.* **1997**, *272*, 14727.
[18] J.-F. Wu, C.-W. Sun, C.-Y. Jiang, Z.-P. Liu, S.-J. Liu, *Arch. Microbiol.* **2005**, *183*, 1.
[19] K. L. Colabroy, H. Zhai, T. Li, Y. Ge, Y. Zhang, A. Liu, S. E. Ealick, F. W. McLafferty, T. P. Begley, *Biochemistry* **2005**, *44*, 7623.
[20] I. Dilović, F. Gliubich, G. Malpeli, G. Zanotti, D. Matković-Calogović, *Biopolymers* **2009**, *91*, 1189.

[21] X. Li, M. Guo, J. Fan, W. Tang, D. Wang, H. Ge, H. Rong, M. Teng, L. Niu, Q. Liu, Q. Hao, *Protein Sci.* **2006**, *15*, 761.
[22] Y. Zhang, K. L. Colabroy, T. P. Begley, S. E. Ealick, *Biochemistry* **2005**, *44*, 7632.
[23] L. Que, Jr., *Biochem. Biophys. Res. Commun.* **1978**, *84*, 123.
[24] A. I. Poddel'sky, V. K. Cherkasov, G. A. Abakumov, *Coord. Chem. Rev.* **2009**, *253*, 291.
[25] H. Chun, E. Bill, E. Bothe, T. Weyhermüller, K. Wieghardt, *Inorg. Chem.* **2002**, *41*, 5091.
[26] H. Chun, C. N. Verani, P. Chaudhuri, E. Bothe, E. Bill, T. Weyhermüller, K. Wieghardt, *Inorg. Chem.* **2001**, *40*, 4157.
[27] H. Chun, T. Weyhermüller, E. Bill, K. Wieghardt, *Angew. Chem.* **2001**, *113*, 2552; *Angew. Chem. Int. Ed.* **2001**, *40*, 2489.
[28] H. Chun, E. Bill, T. Weyhermüller, K. Wieghardt, *Inorg. Chem.* **2003**, *42*, 5612.
[29] K. S. Min, T. Weyhermüller, K. Wieghardt, *Dalton Trans.* **2003**, 1126.
[30] S. Mukherjee, T. Weyhermüller, E. Bill, K. Wieghardt, P. Chaudhuri, *Inorg. Chem.* **2005**, *44*, 7099.
[31] T. K. Paine, S. Paria, L. Que, Jr., *Chem. Commun.* **2010**, *46*, 1830.
[32] Y.-M. Chiou, L. Que, Jr., *J. Am. Chem. Soc.* **1995**, *117*, 3999.
[33] M. M. Bittner, S. V. Lindeman, A. T. Fiedler, *J. Am. Chem. Soc.* **2012**, *134*, 5460.
[34] Y.-M. Chiou, L. Que, Jr., *Inorg. Chem.* **1995**, *34*, 3577.
[35] P. Halder, S. Paria, T. K. Paine, *Chem. Eur. J.* **2012**, *18*, 11778.
[36] D.-H. Jo, Y.-M. Chiou, L. Que, Jr., *Inorg. Chem.* **2001**, *40*, 3181.
[37] T. Ogihara, S. Hikichi, M. Akita, Y. Moro-oka, *Inorg. Chem.* **1998**, *37*, 2614.
[38] H. G. Jang, D. D. Cox, L. Que, Jr., *J. Am. Chem. Soc.* **1991**, *113*, 9200.
[39] M. Y. M. Pau, M. I. Davis, A. M. Orville, J. D. Lipscomb, E. I. Solomon, *J. Am. Chem. Soc.* **2007**, *129*, 1944.
[40] P. Comba, H. Wadepohl, S. Wunderlich, *Eur. J. Inorg. Chem.* **2011**, 5242.